INTERNATIONAL JOURNAL FOR NUMERICAL METHODS IN FLUIDS
Int. J. Numer. Meth. Fluids 2009; **59**:75–89
Published online 2 June 2008 in Wiley InterScience (www.interscience.wiley.com). DOI: 10.1002/fld.1811

Determination of permeability in fibrous porous media using the lattice Boltzmann method with application to PEM fuel cells

Mark A. Van Doormaal and Jon G. Pharoah*, †

Fuel Cell Research Centre and Department of Mechanical and Materials Engineering, Queen's University at Kingston, Kingston, Ont., Canada K7L 3N6

SUMMARY

The lattice Boltzmann method (LBM) is used to simulate the flow through an idealized proton exchange membrane fuel cell (PEMFC) porous transport layer (PTL) geometry generated using a Monte Carlo method. Using the calculated flow field, Darcy's law is applied and the permeability is calculated. This process is applied in both through- and in-plane directions of the paper as both of these permeability values are important in computational fluid dynamics models of PEMFCs.

It is shown that the LBM can be used to determine permeability in a random porous media by solving the flow in the microstructure of the material. The permeability in the through- and in-plane directions is shown to be different and the anisotropic nature of the geometry creates anisotropic permeability. It is also found that fiber arrangement plays a large role in the permeability of the PTL. New correlations are presented for in- and though-plane permeabilities of fibrous porous media with ($0.6<\varepsilon<0.8$). Copyright © 2008 John Wiley & Sons, Ltd.

Received 15 August 2007; Revised 15 February 2008; Accepted 20 February 2008

KEY WORDS: PEM fuel cells; porous media; permeability; numerical methods; lattice Boltzmann method

1. BACKGROUND AND MOTIVATION

Proton exchange membrane fuel cells (PEMFCs) are regarded as the ideal automobile power plant in a hydrogen economy. PEMFCs complete an electrochemical reaction to combine hydrogen and oxygen releasing electricity (and heat), which can be used to do useful work. A simple schematic of such a cell is shown in Figure 1.

*Correspondence to: Jon G. Pharoah, Fuel Cell Research Centre and Department of Mechanical and Materials Engineering, Queen's University at Kingston, Kingston, Ont., Canada K7L 3N6.
†E-mail: pharoah@me.queensu.ca

Contract/grant sponsor: Natural Sciences and Engineering Research Council
Contract/grant sponsor: Queen's-RMC Fuel Cell Research Centre

Copyright © 2008 John Wiley & Sons, Ltd.

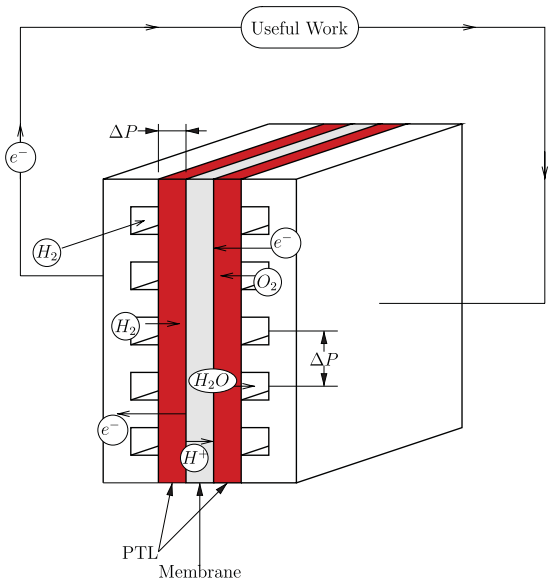

Figure 1. Schematic of a PEM fuel cell.

These fuel cells have been under development for a number of years and work continues on the refinement of their design. A part of the modern design process is computer-aided engineering that includes computer-aided design and computational fluid dynamics (CFD). Work has been done by many researchers to develop full CFD models of PEMFCs including [1–5]. In the case of full three-dimensional PEMFC models, the porous transport layer (PTL) is treated as a homogeneous material with a specified porosity and isotropic transport properties. The PTL is more commonly known as a gas diffusion layer (GDL) and its purpose is to distribute reactants and electrons to and from the catalyst layer, but this term is misleading because in some cases convective transport through this material is critically important to fuel cell performance. Therefore, a name more reflective of their true nature is needed; hence, the less mechanistically restrictive PTL will be used for the remainder of this paper. Figure 2 shows typical serpentine channels that distribute reactant gases to the electrodes. In this arrangement there is a pressure difference between channels and as such a flow can bypass from channel to channel through the PTL. There is also a pressure difference in the direction normal to the PTL due to the consumption of reactants in the fuel cell. These phenomena indicate that permeability, which relates pressure drop to velocity in a porous media, is an important transport property of the PTL. CFD models of PEMFCs use volume-averaging techniques to deal with the PTL. Therefore, the models do not contain pore level detail of the geometry but instead use effective transport properties such as thermal conductivity and permeability. Permeability is defined by Darcy's Law as follows:

$$K = \mu \frac{q}{A} \frac{L}{\Delta P} \tag{1}$$

where K is the permeability, q is the average volume flow rate, A is the cross-sectional area, μ is the viscosity, ΔP is the pressure difference and L is the distance over which the pressure

Copyright © 2008 John Wiley & Sons, Ltd.

DOI: 10.1002/fld

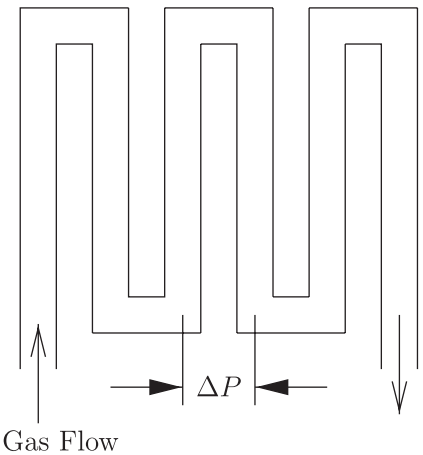

Figure 2. Schematic of a typical PEMFC serpentine flow field.

difference acts. Darcy's law is valid only where the Reynolds number based on the pore size is low ($Re<10$) in the creep flow regime where inertial effects are not important compared with viscous forces [6]. When Darcy's law is extended to three dimensions and expressed in a differential form (Equation (2)), the scalar K becomes a second-order symmetric tensor $\mathbf{K}$ (Equation (3)) and velocity is a vector $\mathbf{u}$ given by

$$\mathbf{u}=-\nabla P\frac{\mathbf{K}}{\mu} \tag{2}$$

$$\mathbf{K}=\begin{bmatrix} K_{11} & K_{12} & K_{13} \\ K_{21} & K_{22} & K_{23} \\ K_{31} & K_{32} & K_{33} \end{bmatrix} \tag{3}$$

Owing to the symmetric nature of permeability, $K_{12}=K_{21}$, $K_{13}=K_{31}$ and $K_{23}=K_{32}$. When the principal axes for permeability are parallel to the coordinate axes, the tensor becomes diagonal. This is not true in general; therefore, the six independent values in the tensor are K_{11}, K_{22}, K_{33}, K_{12}, K_{13} and K_{23}. The physical interpretation of the terms is straightforward and is as follows. K_{ij} is the permeability relating the velocity in the direction i to a pressure gradient in the direction j. Therefore, when the principal axes are not aligned with the coordinate axes, a pressure gradient in one direction can induce a velocity in a perpendicular direction.

The values for permeability in CFD models can make a large difference in predictions of how the cell operates as given in [7, 8] where the flow through the PTL can be seen to heavily depend on the permeability used in the model. Ma *et al.* [9] present a good review of the state of CFD modelling of PEMFCs and state that one of the major challenges in modelling is the knowledge of appropriate material-related transport properties. Both Ma *et al.* and Pharoah *et al.* [10] state that the treatment of the PTL as anisotropic is needed despite the additional complexity it may introduce. Very few PEMFC CFD models consider anisotropic permeability in the PTL but among those that do are Stockie *et al.* [11] and Hakenjos *et al.* [4]. The permeability for these models can

Copyright © 2008 John Wiley & Sons, Ltd.

DOI: 10.1002/fld

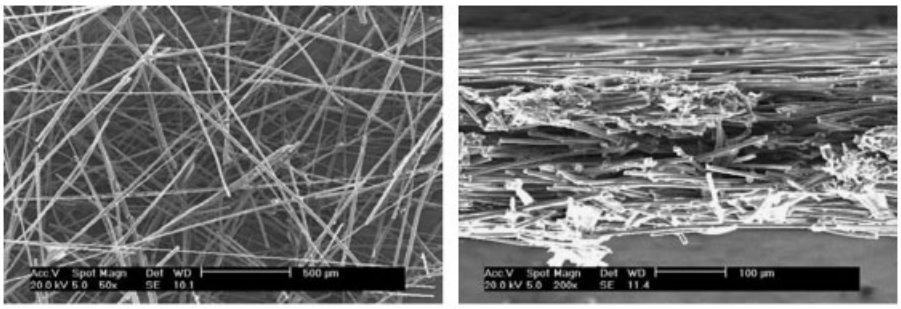

(a) (b)

Figure 3. SEM of a PEM PTL with fibrous micro structure: (a) top/plane view and (b) side/edge view.

be determined by different methods including experimentally or as in this study using a numerical method. Much experimental (see [12–15]) and analytical work (see [16–18]) on permeability of fibrous porous media has been completed and is summarized well by Jackson and James [19]. An accurate value for permeability in the PTL is valuable for those completing CFD studies on PEMFCs and is needed if CFD models are going to be valuable in the fuel cell design process. As well, a tool with the ability to predict the permeability in a given porous geometry could be used in the design process for engineering of the PTL in order to achieve desired performance.

The method used in this study is to simulate flow through a idealized yet representative PTL material using the lattice Boltzmann method (LBM) and using these results to determine permeability by Equation (1). The LBM has been used in porous media studies in the past such as those by Succi *et al.* [20], Inamuro *et al.* [21] and Koponen *et al.* [22].

1.1. The porous transport layer

The PTL is often a carbon-based porous medium that allows for the transport of electrons through the fibers and mass transport in the void space. There are a number of different types of PTL including wet-laid papers, dry-laid papers, carbon fiber cloths and carbon fiber papers. This study concentrates on carbon fiber paper types as they are often used in PEMFCs. Figure 3(a) is a scanning electron micrograph (SEM) of a carbon fiber paper showing a top view. Figure 3(b) is an SEM showing an edge view of the paper. The vertical direction in Figure 3(b) is referred to as the through-plane direction and the vertical and horizontal directions in Figure 3(a) are referred to as in-plane directions. It can be readily seen from these views that the material is anisotropic with a much different structure in the through- and in-plane directions. It can also be seen that the PTL is essentially a set of randomly arranged cylinders with length many times larger than the diameter. These cylinders are arranged in layers stacking in the through-plane direction. The fiber diameter in typical PTLs ranges from about 7 to 12 µm.

The PTL is often treated as an isotropic porous medium despite the fact that the geometry is anisotropic. If the PTL is an orthotropic medium, we would expect that $K_{22} = K_{33}$ (if directions 2 and 3 are the in-plane directions) and in general that $K_{11} \neq K_{22}$. It has also been shown that the choice of permeability used in CFD simulations of PEMFCs has a large impact on the predicted performance of the cells. With this in mind it is important that accurate values for through-plane and in-plane permeabilities are used in CFD simulations in order to obtain accurate results. This is

Copyright © 2008 John Wiley & Sons, Ltd.

DOI: 10.1002/fld

due to the fact that there are pressure gradients in both through- and in-plane directions as shown in Figure 1.

The manufacturing process of these carbon fiber papers is such that there is a preferential fiber direction. The degree to which fibers align in this direction is capable of being modified using the manufacturing process [23]. It is expected that the permeability will depend on the fiber direction.

The purpose of this study is to determine the permeability of idealized yet realistic PTL geometries. The relationships between permeability, porosity, flow direction and fiber arrangement will be explored.

2. THE LATTICE BOLTZMANN METHOD

The LBM has its roots in both cellular automata [24] and the Boltzmann equation [25]. In fact, the LBM can be viewed as a discretized form of the continuum Boltzmann equation [26] and is discretized in terms of space, time, and velocity. It is considered to be a mesoscopic method, not treating the fluid explicitly as a continuum as in Navier–Stokes-based techniques and not as individual particles as with molecular dynamics simulations. Instead, large groups of particles (distributions) move about on a lattice (grid) and collide with each other. At each lattice point, there are a finite number of directions a particle can travel and the particles are grouped according to which direction they can move. There are two steps in the LBM: streaming and collision, and each occurs once per time step. During the streaming step, all particles travel to the neighboring lattice point in the direction of travel. In the collision step, all particles that have arrived at a lattice point collide, conserving mass and momentum. More information on this method and its applicability to fluid mechanics can be found in Succi [27] and Chen and Doolen [28]. The governing equations for the lattice Boltzmann method are given in Equation (4). Note that the following equation contains both streaming and collision steps:

$$f_i(\mathbf{x}+\mathbf{e}_i\Delta x, t+\Delta t) = f_i(\mathbf{x}, t)+\Omega_i(f(\mathbf{x}, t)), \quad i=0, 1, \ldots, M-1 \tag{4}$$

where f_i is the real variable denoting the mass per unit volume of the particles possessing lattice speed i, $\mathbf{e}_i$ is the direction vector for lattice speed i and $M=15$ is the number of lattice speeds used in this study. The direction vector ($\mathbf{e}_i$) used in this study is expressed as

$$[\mathbf{e}_0, \mathbf{e}_1, \mathbf{e}_2, \mathbf{e}_3, \mathbf{e}_4, \mathbf{e}_5, \mathbf{e}_6, \mathbf{e}_7, \mathbf{e}_8, \mathbf{e}_9, \mathbf{e}_{10}, \mathbf{e}_{11}, \mathbf{e}_{12}, \mathbf{e}_{13}, \mathbf{e}_{14}]$$
$$= \begin{bmatrix} 0 & 1 & -1 & 0 & 0 & 0 & 0 & 1 & -1 & -1 & 1 & 1 & -1 & -1 & 1 \\ 0 & 0 & 0 & 1 & -1 & 0 & 0 & 1 & -1 & -1 & 1 & -1 & 1 & 1 & -1 \\ 0 & 0 & 0 & 0 & 0 & 1 & -1 & 1 & -1 & 1 & -1 & 1 & -1 & 1 & -1 \end{bmatrix} \tag{5}$$

This three-dimensional 15-speed model is known as D3Q15 and is used in this study. Other possibilities for three-dimensional lattices include D3Q19 and D3Q27 lattices.

The collision operator Ω_i used here is known as the Bhatnagar–Gross–Krook (BGK) collision operator [29] and it is a single-time relaxation scheme in which all modes (lattice speeds) relax on the same time scale [27]. Specifically, $\Omega_i = -1/\tau(f_i - f_i^{\mathrm{eq}})$, where τ is the relaxation time and f_i^{eq} is the equilibrium distribution.

Copyright © 2008 John Wiley & Sons, Ltd.

DOI: 10.1002/fld

To finish off the definition of the BGK collision operator, the equilibrium distribution needs definition. First, however, the macroscopic field variables density, pressure and the velocity vector (ρ, P and $\mathbf{u}$) need to be determined in terms of the distributions as follows:

$$\begin{aligned} \sum_i f_i^{\mathrm{eq}} &= \sum_i f_i = \rho = 3P \\ \sum_i f_i^{\mathrm{eq}} \mathbf{e}_i &= \sum_i f_i \mathbf{e}_i = \rho \mathbf{u} \end{aligned} \tag{6}$$

The last macroscopic parameter of interest is the viscosity μ, which is defined in terms of the relaxation time (τ) as follows:

$$\mu = \frac{1}{3\rho}\left(\tau - \frac{1}{2}\right) \tag{7}$$

The equilibrium distributions can then be defined in terms of the macroscopic variables according to the following equation:

$$f_i^{\mathrm{eq}} = E_i[1 + 3\mathbf{e}_i \cdot \mathbf{u} + \tfrac{9}{2}(\mathbf{e}_i \cdot \mathbf{u})^2 - \tfrac{3}{2}\mathbf{u} \cdot \mathbf{u}] \quad \text{for } i = 0, 1, \ldots, 14 \tag{8}$$

where $E_0 = \frac{2}{9}$, $E_i = \frac{1}{9}$, $i = 1, 2, \ldots, 6$, and $E_i = \frac{1}{72}$, $i = 7, 8, \ldots, 14$ for the D3Q15 model. The complete set of equations defined above reduces to the Navier–Stokes equations in the low Mach number limit using the Chapman–Engskog expansion as given in [28]. This expansion is also used to arrive at the expression for the vicosity given in Equation (7).

3. METHOD

3.1. Geometry generation

The idealized geometries used in this study were generated using an extension of the Monte Carlo method originally developed by Hamilton [30]. Using the original method the geometry consists of layers of fibers. All of the fibers are parallel in a given layer and are orthogonal to the fibers in neighboring layers. In order to create the geometry each fiber is placed at a random location in the layer such that no fibers overlap but are allowed to touch. This method was used by Hamilton to determine effective diffusive transport coefficients in the PTL. The geometry is generated and simulated as periodic in all directions that eliminates edge effects effectively taking a sample from the middle of a large PTL. A sample geometry generated using this method is shown in Figure 4. The extensions to the original method are now discussed followed by a discussion of the parameter to define these geometries.

The first extension was to create geometries in which the fibers in neighboring layers are parallel. An example of such a geometry is shown in Figure 5.

The second extension was to create geometries in which the angle between fibers in neighboring layers is a value between 0 and 90°. Here, a single fiber is placed at a staring point in a layer and the length is increased until the desired porosity is achieved. The single fiber wraps through the periodic domain. Two different types of geometry were created using this method. In the first the fibers are laid at a random angle (Figure 6) in the layer and in the second fibers are laid at a specified angle in the layer (Figure 7).

Copyright © 2008 John Wiley & Sons, Ltd.

DOI: 10.1002/fld

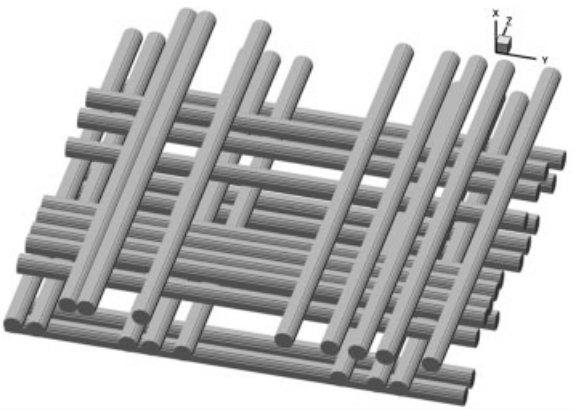

Figure 4. Sample geometry where fibers are orthogonal to fibers in neighboring layers.

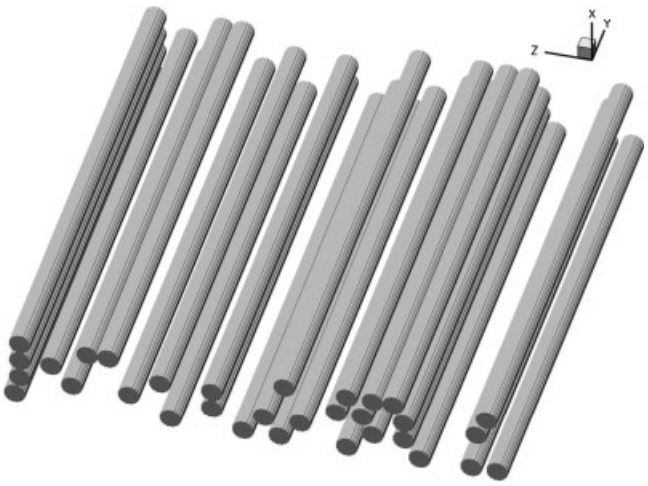

Figure 5. Sample geometry where all fibers are parallel.

We now define the parameter α as the half angle between fibers in neighboring layers. A diagram illustrating the definition of α is shown in Figure 8. For all cases of geometry generation the fibers are arranged in $y-z$ planes. In the case of through-plane flow the mean flow direction is in the x direction and in the case of in-plane flow the mean flow direction is in the y direction. The fibers are arranged at angles $\pm\alpha$ to the y-axis. Therefore, in the case of in-plane flow α is also the angle between the mean flow and the fiber axes. The geometry shown in Figure 4 where fibers in neighboring layers are perpendicular is a case where $\alpha=45°$. The geometry shown in Figure 5 is a case where $\alpha=0°$. Shown in Figure 7 is an example geometry in which $\alpha=60°$.

Once a geometry was created, a pressure difference was imposed in the direction of interest (through- or in-plane) and the flow simulated using the parallel LBM code developed. Once the

Copyright © 2008 John Wiley & Sons, Ltd.

DOI: 10.1002/fld

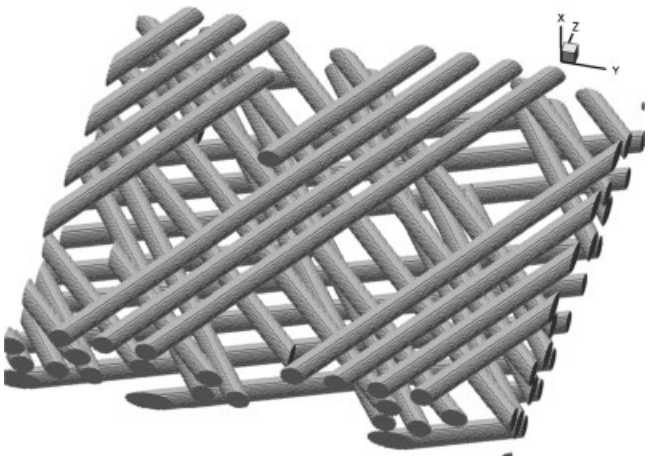

Figure 6. Sample geometry with fibers at random angles.

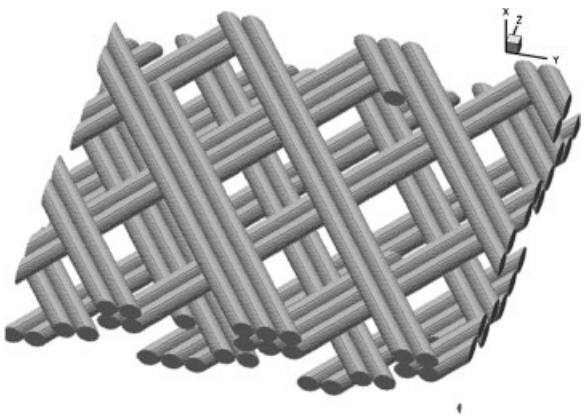

Figure 7. Sample geometry with defined fiber angles ($\alpha = 60°$).

flow reached a statistically stationary state, the flow rate through the domain, in the direction of the pressure gradient, was determined. Then, using Equation (1), the permeability was calculated.

3.2. Verification and validation

The LBM code used in this study was verified by completing simulations on flow situations that have analytical solutions. Specifically, pressure-driven flows in a square channel and between parallel plates were investigated. Both of these situations showed that the method used was second-order accurate as expected and gave good results. In addition, the flow through a periodic array of cylinders was completed and the results compared with those of Kaviany [6]. This step ensured that using a cartesian lattice for round cylinders provided accurate results. Further details of verification and validation can be found in [31].

Copyright © 2008 John Wiley & Sons, Ltd.

DOI: 10.1002/fld

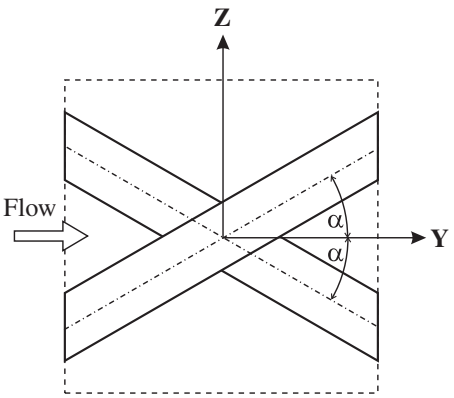

Figure 8. Definition of α.

Twenty-four lattice points per diameter were used in this study, which was determined to be appropriate by simulating the flow around a periodic array of cylinders in parallel and perpendicular arrangements. The size of the domain used in the through-plane study was 12 fiber diameters by 12 fiber diameters per layer and eight layers per sample. The in-plane cases use the same layer size as the through-plane study but only six layers per sample. The domain sizes were determined appropriate by a domain study in which the domain was increased in size until further increases did not cause statistically different results [31].

3.3. Sample-to-sample variability

In order to capture information pertaining to the sample-to-sample variability inherent to random materials, multiple random samples were created at each desired porosity and fiber angle. Between 10 and 15 random samples were run for each case, and the 95% confidence interval determined using student's t-distribution. In the plots below, these 95% confidence intervals are indicated using error bars.

4. RESULTS

A number of different cases were run at four porosites in the range $0.6<\varepsilon<0.81$. The first part of this study is concerned with the relationship between permeability, porosity (ε) and the fiber angle (α). The permeability was determined for $\alpha=0$, 30, 45, 60 and 90° with example geometries shown in Figure 4 ($\alpha=45°$), Figure 5 ($\alpha=0°, 90°$) and Figure 7 ($\alpha=30°, 60°$). The second part of the study includes permeability as a function of porosity for geometries with random fiber angles as shown by example in Figure 6. In terms of the through-plane direction a value of $\alpha=30°$ produces an equivalent geometry to $\alpha=60°$ and a value of $\alpha=0°$ produces an equivalent geometry to $\alpha=90°$; therefore, the fiber angle was set to vary between 0° and 45° for the through-plane study.

The results of a sample solution are shown in Figure 9, which depicts stream tubes through a small portion of the domain for a through-plane flow direction. It is clear from this figure that the flow is both complex and highly three dimensional. As expected the bulk of the flow is channeled through regions of higher porosity while the flow is severely restricted in other areas. In keeping

Copyright © 2008 John Wiley & Sons, Ltd.

DOI: 10.1002/fld

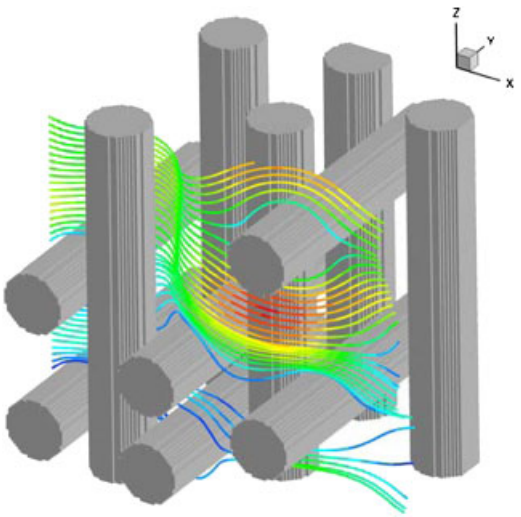

Figure 9. Stream tubes colored by speed in small section of a through-plane domain.

with maintaining the flow in a regime suited to Darcy's law, the Reynolds number was of order 10^{-1}; hence, the flow is in the creeping regime as evidenced by the nearly symmetrical stream tubes around the top right cylinder shown in the figure. Although it would be possible with the current code to increase the Reynolds number and explore the effect of wakes, the purpose of this study was to extract Darcy permeabilities. The investigation of inertial effects will be the subject of a subsequent paper. As mentioned earlier, there are off-diagonal entries in the permeability tensor, which correspond to in-plane pressure gradient causing a through-plane flow and *vice versa*. In all cases these off-diagonal terms were determined, but in all cases very near to zero, and therefore of little consequence.

Figure 10 shows through-plane permeability (non-dimensionalized by fiber radius squared) *versus* porosity for both the LBM results generated in this study and an empirical relationship for the Carman–Kozeny equation [13]. The error bars on the data points indicate the 95% confidence interval using student's t-distribution. The model predictions are compared with the following Carmen–Kozeny equation:

$$K = \frac{\varepsilon^3}{k_k (1-\varepsilon)^2 A_o^2} \tag{9}$$

using a Kozeny constant k_k provided by Ingmanson *et al.* [13] as follows:

$$k_k = \frac{3.5\varepsilon^3 [1+57(1-\varepsilon)^3]}{(1-\varepsilon)^{1/2}} \tag{10}$$

where ε is the porosity, A_o is specific surface area (solid surface area divided by the solid volume) that was calculated by assuming no contact area between cylindrical fibers. This empirical equation was developed for use in the pulp and paper industry for through-plane flow and as should be similar to the present results.

Copyright © 2008 John Wiley & Sons, Ltd.

DOI: 10.1002/fld

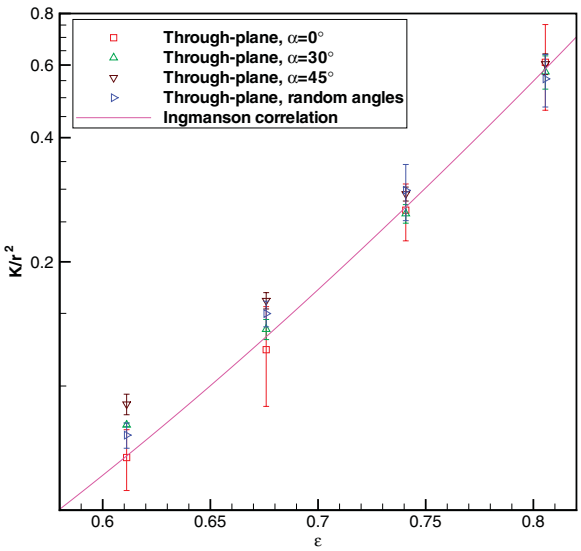

Figure 10. Non-dimensional through-plane permeability *versus* porosity for various fiber arrangements.

The present results are generally in good agreement with the correlation by Ingmanson, with some departure at lower porosity. It is not surprising that the predictions and the correlation deviate at a porosity of 0.61 as the experimental basis was $0.68<\varepsilon<0.96$. For all simulated porosities above 0.65, the results are independent of fiber angle as evidenced by the overlap of the 95% confidence intervals. It can also be noted that the aligned fibers ($\alpha=0°$) result in the largest variability. This result can be explained by the fact that with aligned fibers and the relatively high porosities investigated there will be several flow paths unimpeded by fibers and the frequency of such paths will depend strongly on the random placement of fibers.

Figure 11 shows in-plane permeability *versus* porosity for different fiber arrangements. Both through-plane and in-plane permeabilities depend strongly on the porosity, which is shown by the semi-log plots of Figures 10 and 11. The in-plane results also exhibit a strong dependence on fiber arrangement, with the permeability in general decreasing with increasing α. Within the limits of the 95% confidence intervals, the random fiber arrangements are indistinguishable from $\alpha=45°$ arrangements.

The experimental results of Gostick *et al.* [15] are also shown in Figure 11. Gostick *et al.* undertook an experimental investigation of various commercial PTLs. In this study, the materials were placed in a sample holder and the porosity was varied by increasing the sample compression. Both Darcy permeability and the inertial coefficient were determined in the experiment by measuring the pressure drop as a function of flow rate. One of the tested PTLs, Toray-090, is very similar to the idealized version of the PTL in this study. Gostick *et al.* measured the Darcy permeability of the range ($0.65<\varepsilon<0.8$) and determined a value for the Kozeny constant of 4.07, which is plotted in Figure 11. It is important to note, however, that the first data point at $\varepsilon=0.65$ is notably above the Kozeny curve. In this paper, the porosity varied by adding or subtracting fibers, while in the experimental method, the porosity is varied by subtracting or adding pores. Taking these differences into consideration, the agreement between the predictions and the experiment is very good.

Copyright © 2008 John Wiley & Sons, Ltd.

DOI: 10.1002/fld

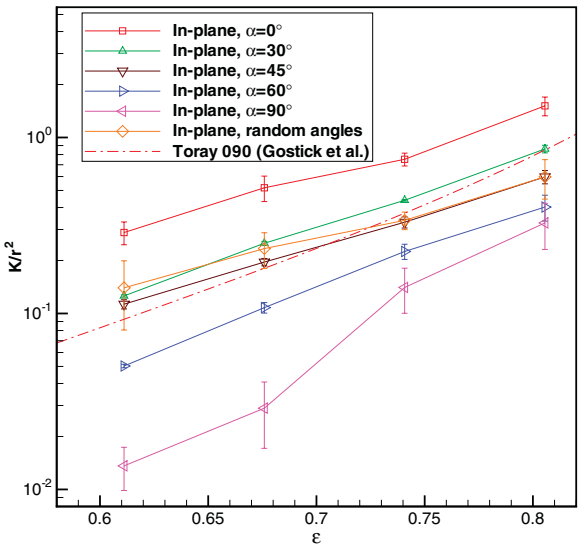

Figure 11. Non-dimensional in-plane permeability *versus* porosity for various fiber arrangements.

The effect of porosity and fiber arrangement on the ratio between in-plane and through-plane permeability ($\chi = K_{\text{in}}/K_{\text{through}}$) is shown in Figure 12. The anisotropic geometries studied here clearly exhibit strongly anisotropic permeability, with the anisotropic ratio tending to unity with increasing porosity. Parallel fibers result in both the largest and the smallest χ values with the smallest being about 0.2 and the largest about 4.2. Using random fiber angles instead of mutually perpendicular fiber layers has a small impact by raising χ at smaller porosity values.

The nature of the manufacturing process of carbon fiber paper PTLs is such that there is a preferential fiber direction; therefore, these results suggest that aligning the fibers in a certain direction would allow us to engineer the performance of the PTL. There are some limits to what can be achieved by angling fibers; for instance, it is possible to increase the ratio between the through-plane and one in-plane permeability, but this occurs at the expense of the other in-plane direction permeability. The work of Pharoah [7] could indicate that an anisotropic in-plane permeability is beneficial. The permeability in the direction of the pressure gradient (see Figure 2) is much more important than the permeability in the orthogonal in-plane direction; hence, the trade-off of decreasing permeability in the other direction may be worthwhile. With this is mind, engineering the PTL by aligning fibers could allow for increased performance in the cell.

For through-plane permeability the correlation in Equation (11) is proposed based on the results of this study. Similarly, the correlation in Equation (12) is proposed for in-plane permeability based on the results of this study. These correlations are based on the form of the equation relating permeability and porosity for an ordered array of cylinders by Sahraoui and Kaviany [32]. Both equations make use of the fiber radius (r).

$$K = 0.28\frac{\varepsilon^{4.3}}{1-\varepsilon}r^2, \quad 0.6 \leqslant \varepsilon \leqslant 0.8 \tag{11}$$

$$K = 0.26\frac{\varepsilon^{3.6}}{1-\varepsilon}r^2, \quad 0.6 \leqslant \varepsilon \leqslant 0.8 \tag{12}$$

Copyright © 2008 John Wiley & Sons, Ltd.

DOI: 10.1002/fld

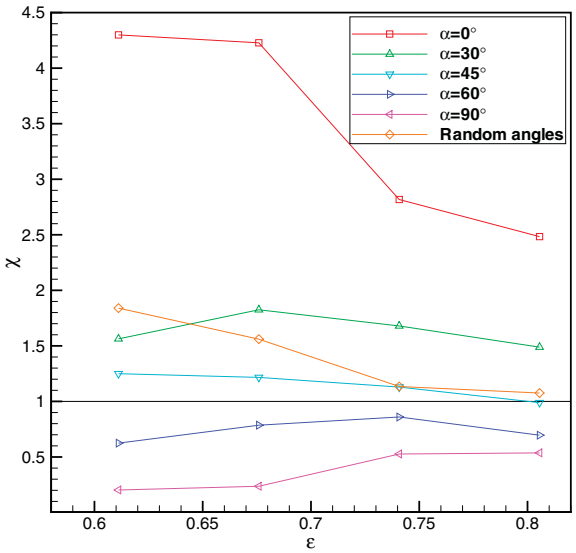

Figure 12. Ratio of in-plane to through-plane permeability *versus* porosity for varying fiber arrangements.

5. CONCLUSIONS

It has been shown that the LBM can be used to determine the permeability in an idealized PTL. The work done in this study characterizes the relationships between permeability, porosity and fiber angle for fibrous porous media. This was done without making many assumptions about the geometry and is based on a numerical experiment based on first principles.

It was shown that the through-plane and in-plane permeabilities depend strongly on the porosity of the sample. The through-plane permeability was not affected much by the fiber angle in contrast to the in-plane permeability, which is greatly affected by fiber angle. When the fibers are aligned with the flow the permeability is at a maximum and when fibers are aligned perpendicular to the flow the permeability is at a minimum. It was also found that the anisotropic microstructure present in the PTL does in fact result in an anisotropic permeability. This is an important result because many researchers are using isotropic permeability values in their CFD models for PEMFCs. When the results for random fiber angles were compared with results in which the fibers in neighboring layers are orthogonal it was found that there was no statistically significant difference in the through-plane directions for porosity greater than 0.61 and no statistical difference in the in-plane permeability. This indicates that the use of perpendicular fibers can be a good approximation of random fiber angles. This result may be of use in future studies of the PTL using this method including multiphase studies and studies concerning the impact of PTFE loading on the permeability. This study in combination with the study by Hamilton [30] in conjunction with good CFD models of a PEMFC could be used to engineer an 'ideal' PTL with anisotropic transport properties that result in an optimal PEMFC performance. In addition to this future use of the study the values for permeability of PTLs can be used immediately in CFD models of the PTL. These values for permeability will increase the accuracy of predictions of the CFD models and could help provide additional insight into PEMFC operation.

Copyright © 2008 John Wiley & Sons, Ltd.

DOI: 10.1002/fld

The present results provide insight into the nature of permeability in fibrous porous media, and as such can provide guidance in the design of engineered materials to achieve specific and directional permeability.

ACKNOWLEDGEMENTS

Financial support from the Natural Sciences and Engineering Research Council is gratefully acknowledged. The authors would also like to thank the Queen's-RMC Fuel Cell Research Centre community for their supports. Computations were carried out using the High Performance Computing Virtual Laboratory housed at Queen's University.

REFERENCES

1. Sivertsen BR, Djilali N. CFD-based modelling of proton exchange membrane fuel cells. *Journal of Power Sources* 2005; **141**:65–78.
2. Wang CY, Wang ZH, Chen KS. Two-phase flow and transport in the air cathode of proton exchange membrane fuel cells. *Journal of Power Sources* 2001; **94**:40–50.
3. Wang L, Husar A, Zhou T, Liu H. A parametric study of PEM fuel cell performances. *International Journal of Hydrogen Energy* 2003; **28**:1263–1272.
4. Hakenjos A, Tüber K, Schumacher JO, Hebling C. Characterising PEM fuel cell performance using a current distribution measurement in comparison with a CFD model. *Fuel Cells* 2004; **4**:185–189.
5. Harvey DBJ. Three-dimensional CFD model for PEMFC cathodes: application to serpentine flow fields. *Master's Thesis*, Queen's University, 2006.
6. Kaviany M. *Principles of Heat Transfer in Porous Media*. Springer: Berlin, 1999.
7. Pharoah JG. On the permeability of gas diffusion media used in PEM fuel cells. *Journal of Power Sources* 2005; **144**:77–82.
8. Yuan J, Rokni M, Sunden B. A numerical investigation of gas and heat transfer in proton exchange membrane fuel cells. *Numerical Heat Transfer Part A* 2003; **44**:255–280.
9. Ma L, Ingham DB, Pourkashanian M, Carcadea E. Review of the computational fluid dynamics modeling of fuel cells. *Journal of Fuel Cell Science and Technology* 2005; **2**(4):246–257.
10. Pharoah JG, Karan K, Sun W. On effective transport coefficients in PEM fuel cell electrodes: anisotropy of the porous transport layers. *Journal of Power Sources* 2006; **161**(1):214–224.
11. Stockie JM, Promislow K, Wetton BR. A finite volume method for multicomponent gas transport in a porous fuel cell electrode. *International Journal for Numerical Methods in Fluids* 2003; **41**:577–599.
12. Davies CN. The separation of airborne dust and particles. *Proceedings of the Institution of Mechanical Engineers* 1952; **B1**:185–198.
13. Ingmanson WL, Andrews RC, Johnson BD. Internal pressure distributions in compressible mats under fluid stress. *Tappi* 1959; **42**:840–849.
14. Ihonen J, Mikkola M, Lindbergha G. Flooding of gas diffusion backing in PEFCs: physical and electrochemical characterization. *Journal of the Electrochemical Society* 2004; **151**:A1152–A1161.
15. Gostick JT, Fowler MW, Pritzker MD, Ioannidis MA, Behra LM. In-plane and through-plane gas permeability of carbon fiber electrode backing layers. *Journal of Power Sources* 2006; **162**(1):228–238.
16. Happel J, Brenner H. *Low Reynolds Number Hydrodynamics*. Martinus Nijhof: Dordrecht, 1986.
17. Brinkmann HC. A calculation of the viscous force exerted by a flowing fluid on a dense swarm of particles. *Applied Scientific Research* 1949; **A1**:27–34.
18. Spielman L, Goren SL. Model for predicting pressure drop and filtration efficiency in fibrous media. *Environmental Science and Technology* 1968; **2**:279–287.
19. Jackson GW, James DF. The permeability of fibrous porous media. *Canadian Journal of Chemical Engineering* 1986; **64**:364–374.
20. Succi S, Cancelliere A, Chang C, Foti E, Gramignani M, Rothman D. A direct computation of the permeability of three-dimensional porous media. *Computational Methods in Subsurface Hydrology*. *Proceedings of the Eighth International Conference on Computational Methods in Water Resources*, Venice, Italy, 1990; 129–136.

Copyright © 2008 John Wiley & Sons, Ltd.

DOI: 10.1002/fld

21. Inamuro T, Yoshino M, Ogino F. Lattice Boltzmann simulations of flows in a three-dimensional porous structure. *International Journal for Numerical Methods in Fluids* 1999; **29**:737–748.
22. Koponen A, Kandhai D, Hellén E, Alava M, Hoekstra A, Kataja M, Niskanen K, Sloot P, Timonen J. Permeability of three-dimensional random fiber webs. *Physical Review Letters* 1998; **80**:716–719.
23. Mathias M, Roth J, Fleming J, Lehnert W. *Fuel Cell Technology and Applications*. Handbook of Fuel Cells: Fundamentals, Technology and Applications, vol. 3. Wiley: New York, 2003.
24. Frisch U, Hasslacher B, Pomeau Y. Lattice-gas automata for the Navier–Stokes equation. *Physical Review Letters* 1986; **56**:1505–1508.
25. Boltzmann L. *Lectures on Gas Theory*. Dover: New York, 1995.
26. He X, Luo L-S. A priori derivation of the lattice Boltzmann equation. *Physical Review E* 1997; **55**(6): R6333–R6336.
27. Succi S. *The Lattice Boltzmann Equation for Fluid Dynamics and Beyond*. Oxford University Press: Oxford, 2001.
28. Chen S, Doolen G. Lattice Boltzmann method for fluid flows. *Annual Review of Fluid Mechanics* 1998; **30**:329–364.
29. Bhatnagar PL, Gross EP, Krook M. A model for collision processes in gases. I: small amplitude processes in charged and neutral one-component system. *Physical Review* 1954; **94**:511–525.
30. Hamilton D. A numerical method to determine effective transport coefficients in porous media with application to PEM fuel cells. *Master's Thesis*, Queen's University, 2005.
31. Van Doormaal M. Determination of permeability in fibrous porous media using the lattice Boltzmann method with application to PEM fuel cells. *Master's Thesis*, Queen's University, 2006.
32. Sahraoui M, Kaviany M. Slip and no-slip velocity boundary conditions at interface of porous, plain-media. *International Journal of Heat and Mass Transfer* 1992; **35**:927–943.

Copyright © 2008 John Wiley & Sons, Ltd.

DOI: 10.1002/fld